Supporting Information

An acoustofluidic chemical waveform generator and switch

Daniel Ahmed,[a] *Hari S. Muddana,*[b] *Mengqian Lu,*[a] *Jarrod B. French,*[c] *Adem Ozcelik,*[a] *Ye Fang,*[d] *Peter J. Butler,*[b] *Stephen J. Benkovic,*[c] *Andreas Manz,*[e] *and Tony Jun Huang*[*a]

[a]Department of Engineering Science and Mechanics, The Pennsylvania State University, University Park, Pennsylvania 16802, USA. Tel: 814-863-4209; Fax: 814-865-9974; E-mail: junhuang@psu.edu

[b]Department of Bioengineering, The Pennsylvania State University, University Park, PA 16802, USA.

[c]Department of Chemistry, The Pennsylvania State University, University Park, PA 16802, USA.

[d]Biochemical Technologies, Science and Technology Division, Corning Corporation, Corning, New York, 14830 USA.

[e]Korean Institute of Science and Technology (KIST) in Europe, Campus E71, D-66123, Saarbruecken, Germany

***Corresponding Author**: E-mail: junhuang@psu.edu; Fax: 814-865-9974; Tel: 814-863-4209

Design and dimensions of the microchannels

Fig. S1 shows two images of the horse-shoe structure (HSS). Fig. S2 shows the 3 x 3 array of HSS used to prescreen the appropriate dimensions of the two HSSs that were later utilized in the chemical switching device. Fig. S3 shows the design and dimensions of the microchannels used for (a) chemical waveform generation and (b) switching.

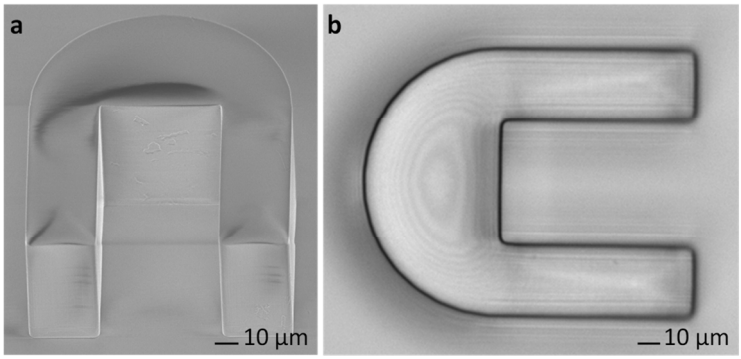

Supplementary Figure S1 | (a) An SEM image of the HSS within the PDMS microfluidic channel. (b) Optical image showing the top view of the HSS structure.

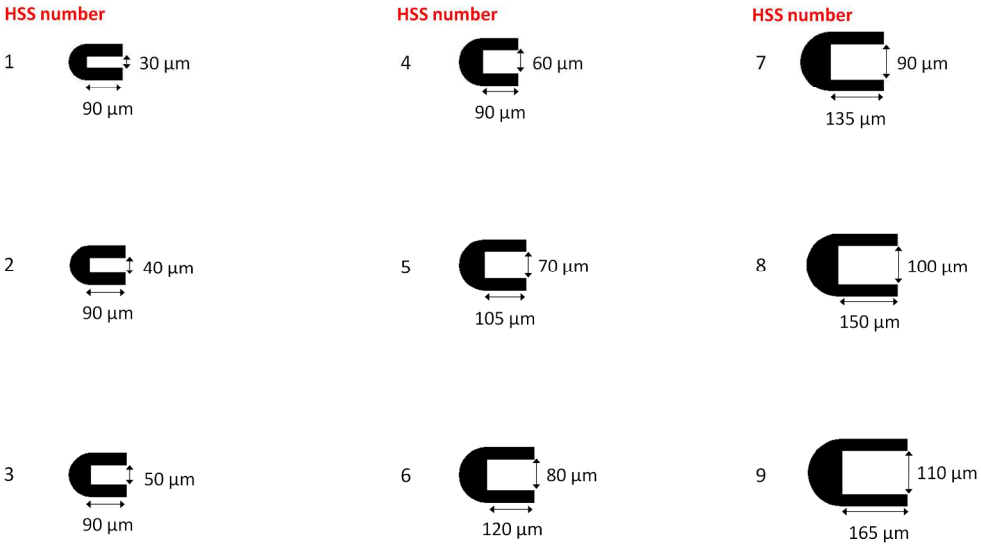

Supplementary Figure S2 | The 3 x 3 array used to prescreen the resonance frequencies of the HSSs to prevent cross-excitation in the chemical switching experiment.

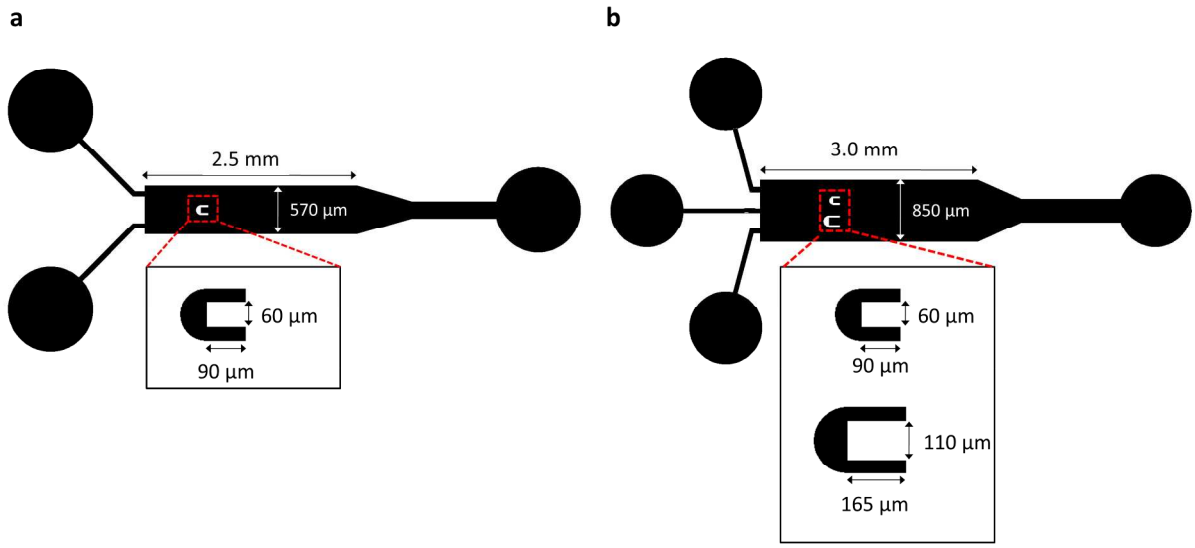

Supplementary Figure S3 | Design and dimensions of the microchannels used for (a) chemical waveform generation and (b) switching.

Optimized flow rate for bubble trap

The outlet flow rates were optimized to achieve repeatable bubble traps within the HSS (listed in Table S1).

Device	Flow rate
1 bubble	6 µl/min
3 x 3 array of HSS	12 µl/min
2 bubble	12 µl/min

Supplementary Table S1 | Optimized flow rates for repeatable bubble traps within the HSS.

Input signals given to the piezoelectric transducer

Fig. S4 shows the electrical signals applied to the piezoelectric transducer by the function generator driving at the resonance frequency of the bubble.

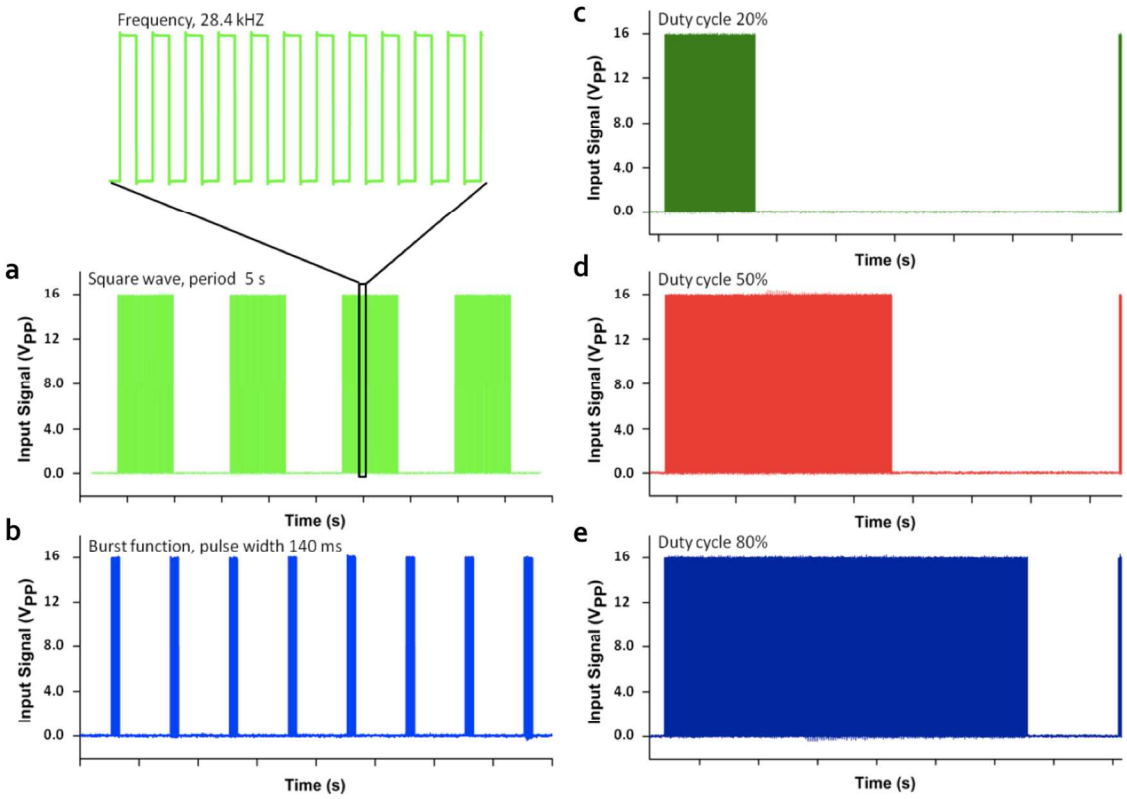

Supplementary Figure S4 | Input signal given to the piezoelectric transducer by the electrical function generator, driving at the resonance frequency of the bubble (see inset) for (a) Square wave generation. (b) Burst cycle generation. (c–e) 20, 50, and 80% duty cycle.

Interface shift

As the flows rates from the two fluids change in the microchannel, the location of the interface between the two fluids shifts along the width of the channel due to the difference in inlet pressures.

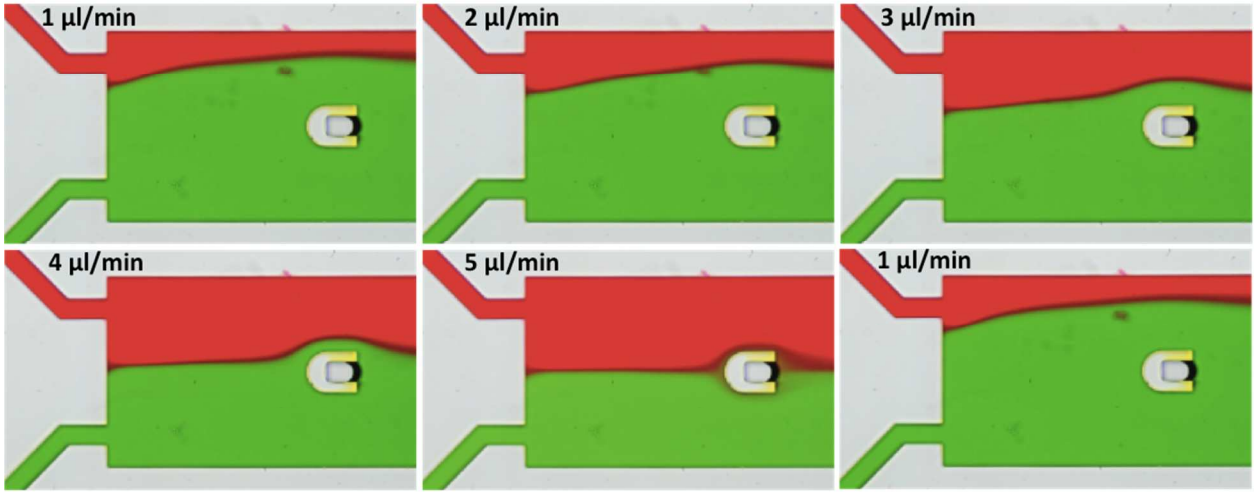

Supplementary Figure S5 | Image sequence showing the shift of interface by flow rate applied in Fig. 2e in the main text but with no mixing.

Characterization of bubbles' resonance frequencies

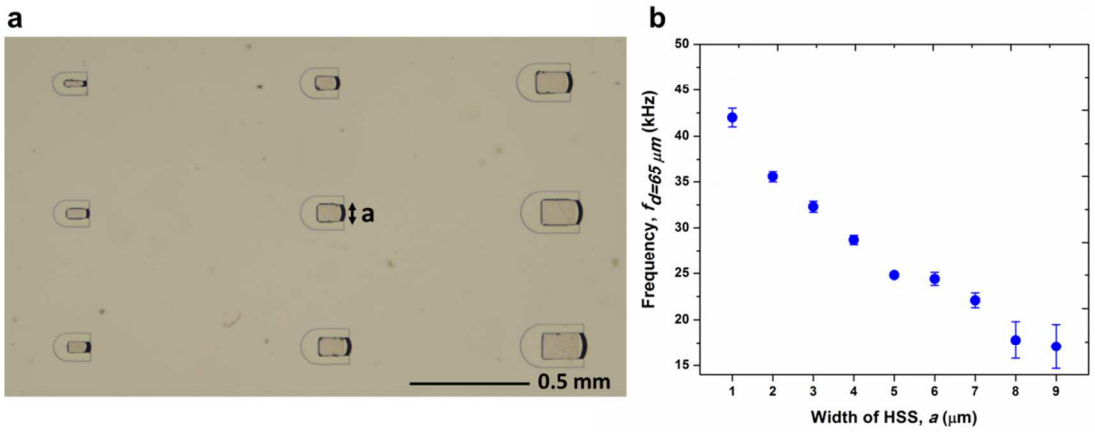

Supplementary Figure S6 | Characterization of bubbles' resonance frequencies. (a) A 3 x 3 array of HSSs with different dimensions used to obtain different sized bubbles. (b) Graph of the experimental results for resonance frequencies of different-sized bubbles. Error bars represent the standard deviation from three measurements conducted from three different microfluidic chips with depths of 65 μm.

Dynamic mass redistribution (DMR) assay

Label-free DMR assays enabled by RWG biosensor were performed using Corning® Epic® BT system, a swept wavelength interrogation system that is capable of imaging whole RWG biosensor microplates with a spatial resolution of 90 μm (1, 2). This system uses a light beam from a tunable light source to illuminate whole 384 well biosensor microplates, and a high-speed complementary metal-oxide semiconductor (CMOS) digital camera to record the escaped and reflected resonant lights from the whole plate. The tunable light source sweeps the wavelength range from 825 to 840 nm in a stepwise fashion to identify the resonant wavelength at each location. A total of 150 spectral images were acquired within a single sweeping cycle (3 sec), and were then processed into a sensor resonant wavelength or DMR image in real time.

For receptor signaling, cells were first harvested from T75 flasks using trypsin/ethylenediamine-tetraacetic acid, and re-suspended in the completed medium. Cells were seeded onto the fibronectin-coated biosensor microplates using a seeding density of 12,000 cells per well in 40 μl complete medium, and cultured at 37°C with 5% CO_2 inside a cell culture incubator for about 22 hours to reach a confluency of ~95%. Afterwards, the cells were washed three times using a plate washer (Bio-Tek Microplate Washers ELx405™, Bio-Tek, Winooski, VT), and maintained in the assay buffer (HBSS) for about one hour to reach equilibrium at 26^{o}C. After establishing a 2 min baseline, DMR assays were then initiated by adding the HBSS-buffered compound solution and the compound-induced DMR was recorded in real time.

Results showed that epinephrine gave rise to a single EC_{50} of 11.4±1.2 nM (n = 4) in the parental cells (Fig. S6). In contrast, the engineered cells epinephrine displayed an assay time dependent potency; that is, the potency to reach the early peak response was found to be biphasic with two well-separated EC_{50} (0.58±0.04 nM, and 69.5±7.1 nM, respectively), while the potency

to reach the late plateau response was monophasic with an EC_{50} of 124±11 nM (Fig. 6). Nonetheless, these results suggest that when overexpressed in HEK293 cells the β_2AR-GFP is functional.

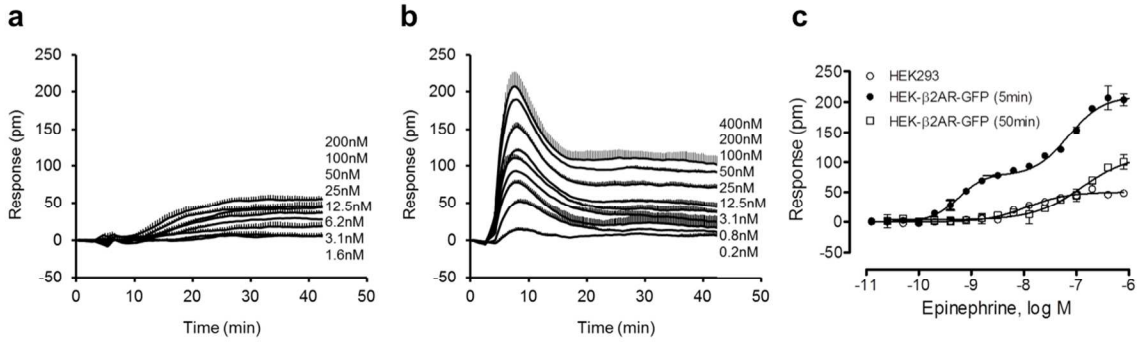

Supplementary Figure S7 | DMR characterization of the β_2-ARs. (a, b) The real-time DMR signals of epinephrine at different doses in (a) the parental HEK293 cells; (b) the HEK-β_2AR-GFP cells; (c) the dose-dependent DMR amplitudes of epinephrine in both cell lines. For the parental HEK cell line which endogenously expresses the β_2-ARs at low level, the DMR amplitude at 50 min post stimulation was plotted. For the HEK-β_2AR-GFP cells the DMR amplitudes at both 5 min and 50 min post stimulation were analyzed. For (a-c), the data represents mean ± s.d. (n =4).

Movie captions

Supplementary Movie 1: "Single bubble trap" (157 KB)

Green dye was infused into the channel outlet at 6 µl/min by a syringe pump. This flow rate allowed us to repeatedly trap a bubble only within the HSS. The video is captured by a Nikon D3S at 24 fps.

Supplementary Movie 2: "Multiple bubble traps" (334 KB)

Green dye was infused into the channel outlet at 12 µl/min by a syringe pump. This flow rate allowed us to repeatedly trap two bubbles within the HSSs. The video is captured by a Nikon D3S at 24 fps.

Supplementary Movie 3: "Mixing of red and blue food dye" (197 KB)

High-speed video showing the rapid mixing of red and blue dyes by bubble oscillation. The video was captured by Casio EX-F1 at 1200 fps.

Supplementary Movie 4: "Larger bubble excitation" (2,058 KB)

Chemical switching device with inlets 1 and 3 containing red and blue dyes with a flow rate of 2 µl/min, and the central region containing water flowing at 4 µl/min. A single bubble was excited at 14.7 kHz, which consequently mixed the red dye with water filling the region of interest.

Supplementary Movie 5: "Smaller bubble excitation" (2,058 KB)

Chemical switching device with inlets 1 and 3 containing red and blue dyes with flow rates of 2 µl/min, and the central region containing water flowing at 4 µl/min. A single bubble was excited at 29.5 kHz, which consequently mixed the red dye with water filling the region of interest.

Supplementary Movie 6: "Chemical binary switch" (1,659 KB)

A video demonstrating switching between the red and blue dyes, achieved by programming the piezoelectric transducer to alternate between two excitation frequencies.

References

1. Ferrie LD, Wu Q and Fang Y (2010) Resonant waveguide grating imager for live cell sensing. *Appl. Phys. Lett.* 97:223704.

2. Fang Y (2011) The development of label-free cellular assays for drug discovery. *Expert Opin. Drug Discov.* 6(12):1285-1298